JGR Atmospheres

RESEARCH ARTICLE
10.1029/2019JD032151

Constraints on Recoil Leader Properties Estimated from X-ray Emissions in Aircraft-Triggered Discharges

C. A. Skeie[1], N. Østgaard[1], N. G. Lehtinen[1], D. Sarria[1], P. Kochkin[1], A. I. de Boer[2], M. Bardet[2], C. Allasia[3], and F. Flourens[3]

[1]Birkeland Centre for Space Science, Institute of Physics and Technology, University of Bergen, Bergen, Norway, [2]Royal Netherlands Aerospace Centre, Amsterdam, Netherlands, [3]Airbus, Toulouse, France

Key Points:
- Observations of 54 X-ray bursts associated with recoil events during aircraft-triggered lightning are presented
- Using three models, we find constraints to the gap and leader length of the recoil events
- We find that the gap length is restricted from 1 to 93 m and the leader length is from 1 to 240 m

Correspondence to:
C. A. Skeie,
Chris.Skeie@uib.no

Citation:
Skeie, C. A., Østgaard, N., Lehtinen, N. G., Sarria, D., Kochkin, P., de Boer, A. I., et al. (2020). Constraints on recoil leader properties estimated from X-ray emissions in aircraft-triggered discharges. *Journal of Geophysical Research: Atmospheres*, *125*, e2019JD032151. https://doi.org/10.1029/2019JD032151

Received 3 DEC 2019
Accepted 9 JUN 2020
Accepted article online 10 JUN 2020

Abstract During Airbus aircraft campaigns flying into thunderstorms in 2014–2016, X-rays were observed during two stages of aircraft-triggered lightning: nanosecond pulses of X-rays associated with negative leader steps and bursts of X-rays during recoil events. This work will focus on the observations of X-ray bursts associated with recoils. Recoils are observed as microsecond-fast changes in the local electric field, associated with large currents passing through the aircraft, and are found to sometimes be associated with bursts of X-rays. From over 200 aircraft-triggered lightning strikes, 54 recoil events were found to be associated with microsecond bursts of X-rays. The majority of the bursts consist of 1–3 X-ray pulses, with some bursts containing as many as 29 X-ray pulses. We compare the observed superposed X-ray spectrum with modeled spectra using a GEANT4 model of the detector and aircraft, to determine the source potential needed to accelerate the electrons that produce the observed X-rays. A model of the recoil leader was made to determine the gap distance and gap potential between the recoil leader and the aircraft. From the modeling, we determine a solution space for the gap and leader lengths where the gap length is constrained by the observed minimum and maximum times between the onset of the X-ray pulses and the onset of the current pulses detected at the aircraft (1 to 93 m). We also find two constraints from the fitting of the modeled spectra to the superposed spectrum, limiting the leader length to between 1 and ~240 m.

1. Introduction

Most lightning strikes to aircraft are not intercepted but triggered by the aircraft itself. The triggering of a lightning strike happens as the aircraft enters a sufficiently large ambient electric field, such as those found in thunder clouds. In the presence of the ambient electric field, the aircraft will be polarized, and the local electric field on the aircraft and its vicinity will become amplified. The sharper parts of the aircraft (nose, tail, and wing tips) will experience the most intense amplifications, as they will enhance the electric field the most. This intensification can lead to the triggering of a lightning discharge from the aircraft. The triggered lightning will consist of a bidirectional leader originating from the aircraft. Commonly, the bidirectional leader will start with a positive leader initiating at one extremity of the aircraft, which propagates in the direction of the ambient electric field. This will further polarize the aircraft, and a negative leader will shortly after be initiated at a different extremity, which will propagate in the opposite direction of the ambient electric field. The bidirectional leaders may then connect to oppositely charged regions in the thunderclouds and trigger a lightning flash, with the aircraft as part of the lightning channel (Mazur, 1989a).

There have been four major airborne lightning-characterization studies that have laid the groundwork for our understanding of the aircraft-lightning relationship. These are as follows: Rough Rider project in the 1960s, NASA's Storm Hazards Program, the Lightning Characterisation Program, and the Transall Program in the 1980s. These four programs collected data on the various stages of thunderstorms, lightning attachment points and current measurements on the aircraft during lightning strikes, ambient and local electric field measurements, X-ray measurements, and optical observations (Fisher et al., 1988; McCarthy & Parks, 1985; Miller, 1968; Parks et al., 1981; Uman & Rakov, 2003). There has also been three aircraft campaigns (ALOFT, ADELE, and ILDAS) dedicated to the study of high-energy emissions from lightning and thunderclouds, such as terrestrial gamma-ray flashes (TGFs), gamma-ray glows, and X-rays generated

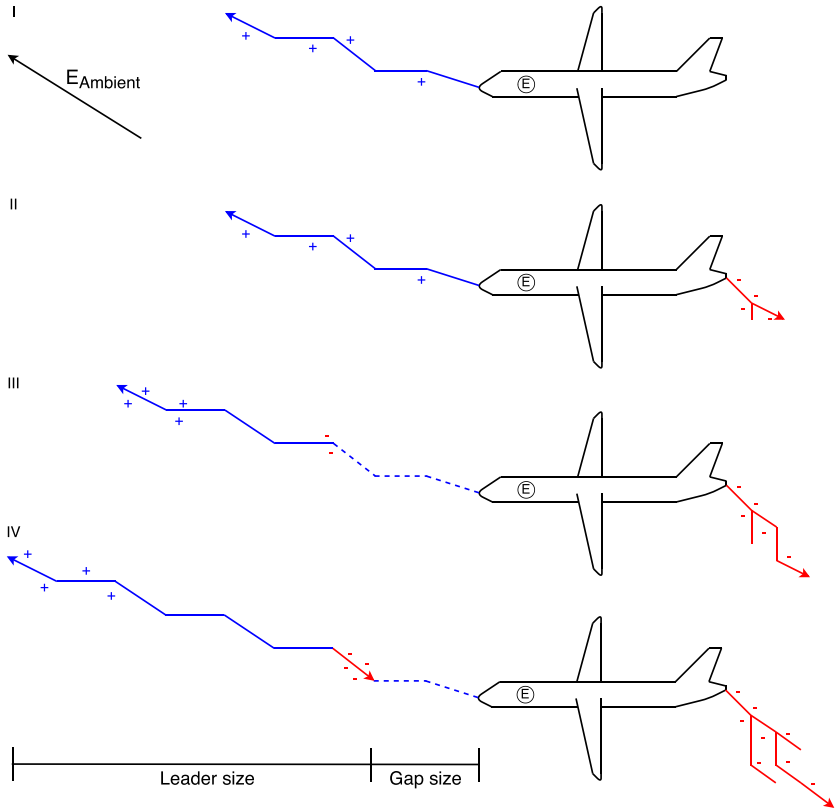

Figure 1. Figure illustrating the initiation of an aircraft-triggered lightning strike and the formation of a recoil leader. (I) The aircraft initiates the positive leader (blue line) after becoming charged and polarized. (II) A few milliseconds later, the negative leader (red line) is launched from an opposite extremity of the aircraft. (III) Tens of milliseconds later, after the current cutoff, the positive leader will continue to propagate, while the lower end (dotted blue line) will cool down and lose conductivity. The leader will obtain induced charges, which will be distributed as a dipole. (IV) The induced charges may lead to negative electric breakdown at the lower end of the positive channel, initiating an ionization wave, which will form a negative recoil leader (red arrow on the left side of the aircraft), which will propagate back toward the aircraft inside the cooled channel (Mazur & Ruhnke, 1993).

during aircraft-triggered lightning strikes (Dwyer et al., 2012; Kelley et al., 2015; Kochkin et al., 2015, 2017, 2018; Østgaard et al., 2019).

In the early 2000s, it was discovered that both natural and triggered lightning can generate microsecond-fast bursts of X-rays (Dwyer, 2004, 2003; Dwyer et al., 2004, 2005, 2011; Howard et al., 2010; Kochkin et al., 2015; Montanyà et al., 2014; Moore et al., 2001; Saleh et al., 2009; Schaal et al., 2012). The observed energies of the bursts are typically in the range of a few hundreds of keV. The bursts of radiation have since been tied to the stepping of negative leaders and to the so-called recoil events during a lightning flash.

According to Mazur (2002) and Mazur et al. (2013), recoil events are a collective term for dart and recoil leaders observed during a lightning flash. During recoil events, large currents pass through an already existing leader channel. These events are some of the most luminous and noticeable parts of a lightning flash. Ogawa and Brook (1964) suggest that the events known as K-changes are negative recoil leaders occurring when a positive leader propagates into a negative charge in a cloud. From analysis of aircraft-triggered lighting flashes, it was hypothesized that recoil leaders are initiated when the positive part of a bidirectional leader extends into a region of negative charge, where an ionizing wave will initiate and propagate back toward the aircraft, along the channel of the preceding positive part of the bidirectional leader attached to the aircraft. The mechanism for the occurrence of a recoil leader is still unknown. Figure 1 shows an illustration of the steps from lightning initiation to recoil leader formation, which we observe in most aircraft-triggered lightning strikes. In Step I, the aircraft has entered a thundercloud, been polarized, and initiated a positive leader. The positive leader will travel in the direction of the ambient electric field and causes negative charge to

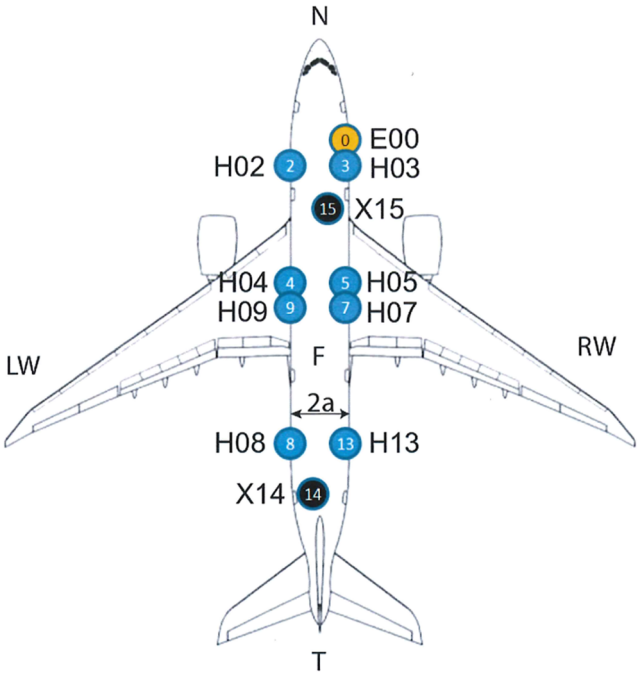

Figure 2. Distribution of the ILDAS instruments on board the Airbus aircraft in 2014 to 2016. The sensor named E00 is the onboard local electric field sensor, HXX sensors are the H-field sensors, and the XXX sensors are the X-ray sensors. Image from Kochkin et al. (2015).

accumulate on the aircraft. Step II happens a few milliseconds after Step I, when the aircraft launches a negative leader from a different extremity. The negative leader will propagate in the opposite direction of the ambient electric field and remove negative charge from the aircraft. Step III happens tens of milliseconds later, after the current cutoff. Now the positive leader channel continues to extend away from the aircraft, while the connected end cools down and loses conductivity, all the while maintaining its net positive charge. The positive leader will obtain induced charges, which will be distributed as a dipole. Step IV shows how the charging may lead to negative electrical breakdown at the active part of the positive leader end close to the aircraft, initiating an ionizing wave, which forms the negative recoil leader. This negative recoil leader will propagate backwards through the cooled channel, until it reaches the origin of the positive leader (the aircraft) (Kochkin et al., 2015; Lalande et al., 1999; Laroche et al., 2012; Mazur, 1989a, 1989b; Mazur & Moreaut, 1992; Mazur & Ruhnke, 1993; Moreaut et al., 1992).

In this paper, we will report observations of X-rays associated with lightning recoil events during aircraft-triggered lightning and use these observations to define a constraint on recoil leader properties.

2. Instruments and Data

During 2014–2016, three thunderstorm-penetrating aircraft campaigns were conducted by Airbus. The aircraft was equipped with the In-flight Lightning Damage Assessment System (ILDAS) (Royal Netherlands Aerospace Centre, 2015), which consisted of one local electric field sensor, two X-ray detectors, and eight H-field detectors, distributed as shown in Figure 2. The system was created by the Royal Netherlands Aerospace Centre in collaboration with 12 partners to measure lightning flash parameters and to determine lightning leader entry and exit points on the aircraft. This system is extensively described in Boissin et al. (2012), Deursen (2011), de Boer et al. (2011), de Boer, Boissin, et al. (2013), de Boer, Bardet, et al. (2013, 2015), van Deursen et al. (2013), Herv et al. (2014), and Zwemmer et al. (2009).

Both the E- and H-field detectors are differential detectors with a frequency band from 10 Hz to 500 kHz for the E-field sensor and 100 Hz to 50 MHz for the H-field sensor. Both sensors have a sampling rate of 83.3 MHz, which corresponds to a sampling interval of 12 ns. The main purpose of the E-field sensor is to act as a trigger for data recording during lightning flashes. The E-field sensor is mounted on the edge of a window toward the front of the aircraft, where it enhances the local electric field over the homogeneous electric field of the fuselage. As the local electric field signal is time differentiated, the zero value for the electric field is of an unknown magnitude. The polarity of the E-field sensor signal is chosen such that a positive signal corresponds to electric field lines pointed toward the detector (Kochkin et al., 2015). The H-field sensors are used to find the current passing through the hull of the aircraft. Six of the detectors are set up to measure the current passing from nose to tail, and sensors H04 and H05 measure the current entering the main fuselage from the wings. The X-ray detectors consist of two cylindrical $LaBr_3(Ce)$ scintillators of $38 \times 38\ mm^2$ size, connected to photomultipliers. The photomultiplier has a rise time of 11 ns, during which we cannot distinguish single photons. The sampling rate of the X-ray detectors is 100 MHz, which corresponds to a sampling interval of 10 ns. The X-ray detectors can measure up to 10 MeV, but the sensitivity of the instrument decreases from ~550 keV, as seen in Figure 10 in Kochkin et al. (2018).

The measurements are continuously stored in a 1.2 s ring buffer memory. When a lightning flash occurs, the local electric field sensor will trigger, and data will be collected and saved for all the sensors for a period of 0.2 s before the trigger and up to 1 s after the trigger. Most data used in this paper were obtained from the 2014–2015 campaigns, consisting of 9 days where the aircraft flew into thunderclouds at an average altitude of 4 km over southern Europe and the Mediterranean Sea. Six X-ray-producing recoil events were also found in the 2016 campaign data, consisting of 6 days where the aircraft flew at 10 km altitudes over northern Australia.

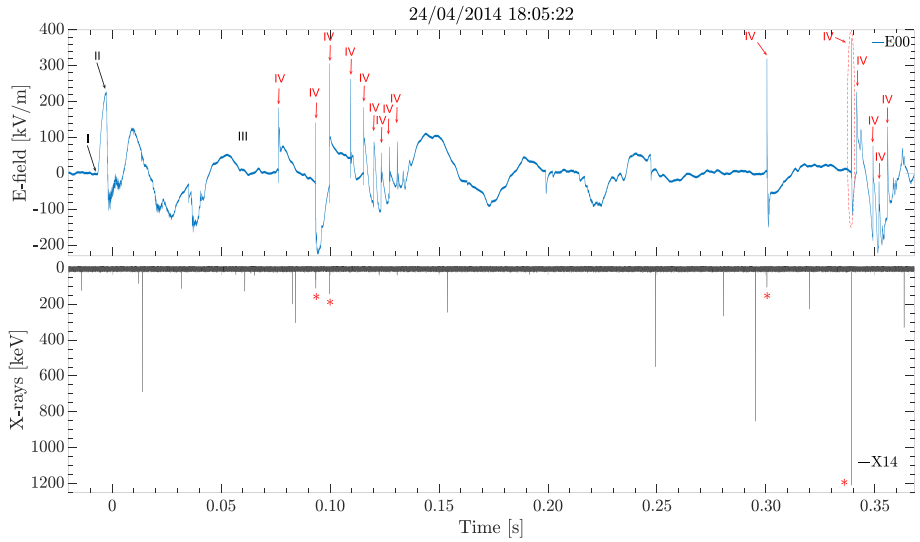

Figure 3. (Top panel) Local electric field measurements during the aircraft-triggered lightning on board the aircraft. The number I and II arrows show when the positive and negative lightning leaders are initiated, the number III arrow indicates the time of the current cutoff, and the red arrows show 15 recoil events. The dotted red ellipse shows a recoil event with associated X-ray burst. (Bottom panel) X-ray measurements during the aircraft-triggered lightning, with red asterisks showing nonbackground X-ray bursts.

3. Observations

During the ILDAS campaign, over 120 aircraft-triggered lightning strikes were observed over 15 days. Figure 3 shows the local electric field signature and accompanying X-ray measurements of one of these aircraft-triggered lightning strikes, with numbers indicating the different steps, as shown in Figure 1. The lightning strike is initiated as the positive leader is launched (I), which results in the local electric field increasing as the aircraft accumulates negative charge. A few milliseconds later, the negative leader is initiated (II), followed by a decline in the local electric field. Approximately 80 ms later, after the current cutoff (III), the first of 15 recoil processes are seen (red IVs) as a fast and large pulse in the local electric field, caused by the wave of negative charges passing through the aircraft. In the bottom panel, 12 background bursts with X-ray energies over 50 keV and multiple with lower energy can be seen. We define background as any count without an associated change in the local electric field. The red asterisks show the X-ray bursts associated with changes in the local electric field during the aircraft-triggered lighting strike. The majority of these background events stem from cosmic-ray background, but some are also from the radioactivity of the scintillation crystal. The background counts are heavily dependent on the flight altitude, with average values of 37 and 45 background counts per second for the 2014 and 2015 campaigns.

The recoil event marked with the dotted red ellipse is shown with a finer timescale in Figure 4. The top panel shows a ~400 kV/m change in local electric field caused by the sudden influx of negative charge from the recoil leader. The middle panel shows the currents passing through the aircraft as the recoil leader connects to the aircraft. The bottom panel shows the associated burst of five X-ray pulses. The dotted red lines show the delay of ~0.6 μs between the onset of the X-ray observations and the onset of the current pulse. This type of delay was manually identified for all the recoil processes that had associated bursts of X-rays and were found to vary from 0.1 to 9.3 μs with a mean of 1.75 μs.

During the test flights, a total of 54 recoil events were found to be accompanied by detectable X-ray bursts. These recoil events produce microsecond-fast bursts of multiple nanosecond-fast X-ray pulses. The majority of these bursts consists of 1–3 pulses, but some were found to contain as many as 29 pulses. Due to instrumental limitations, the nanosecond-fast X-ray pulses can consist of multiple X-ray photons. The recoil events are all associated with large (average of 240 kV/m) changes in the local electric field, happening on a scale of microseconds, and with large (hundreds to thousands of amperes) long-lasting (microseconds long) current pulses flowing over the aircraft body. From the 54 observed recoil events, we identified 245 individual

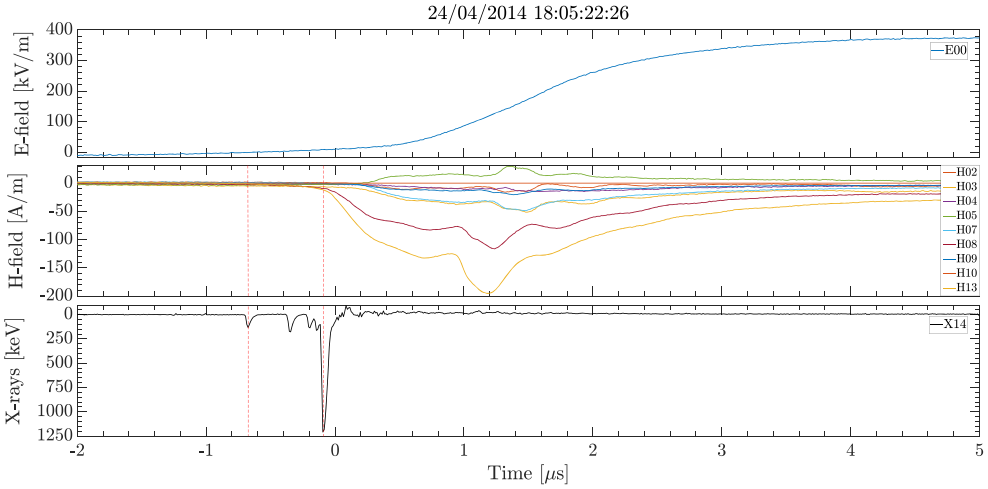

Figure 4. (Top panel) Local electric field signature of connecting recoil leader as observed on the aircraft. Electric field is plotted in such a way that a positive signal corresponds to electric field lines pointed toward the detector. (Middle panel) Measurements of the current passing through the aircraft fuselage during the recoil event. (Bottom panel) Associated X-ray burst, consisting of five pulses lasting approximately 1 μs. The dotted red lines show the onset of the X-ray burst and the onset of the current pulses.

nanosecond pulses of X-rays. Out of the 245 ns pulses, 175 of them were observed before the current wave entered the aircraft. The X-rays produced after the current entered the aircraft are believed to be produced at different extremities of the aircraft by sparks, created by the change in surface potential on the aircraft by the connecting recoil leader. The full width at half the maximum of the X-rays pulses were then compared to each other and to a ^{137}Cs calibration source of 662 keV photons. Pulses with widths found to be over 25% broader than the calibration pulse were removed (19 such pulses were found), as they likely consist of multiple X-rays of lower energies. Figure 5 shows the energy spectra of the nanosecond X-ray pulses observed before the current wave enters the aircraft. As observed, there is a cutoff at 500 keV, which is a real cutoff, as the X-ray detectors can measure energies up to 10 MeV. The error bars are calculated as the square root of the counts of each bin of the spectrum. A bootstrapping method applied to the same modeled spectra (not shown) also gave the same error bars, except for the last two bins where they were a bit larger with the bootstrapping method.

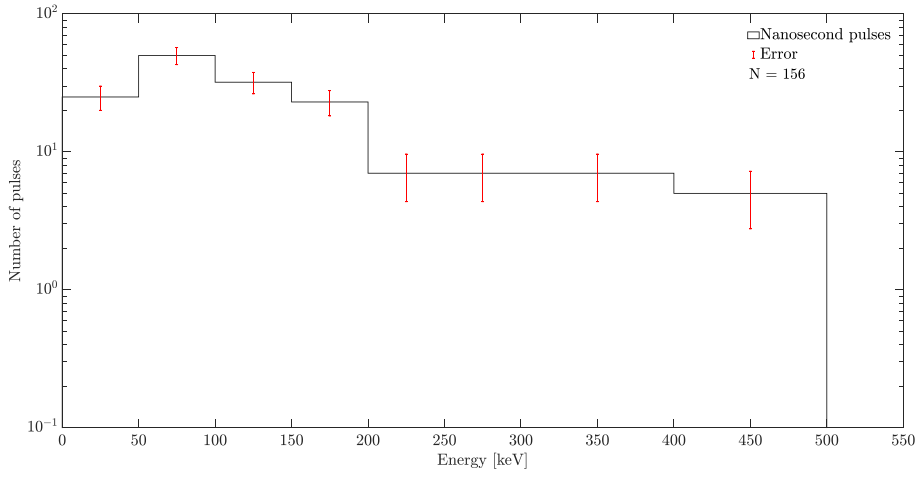

Figure 5. Superposed spectrum of 156 X-ray pulses associated with recoil processes in aircraft-triggered lightning, binned to 50 keV from 0 to 300, and 100 keV bins from 300 to 500, with error bars.

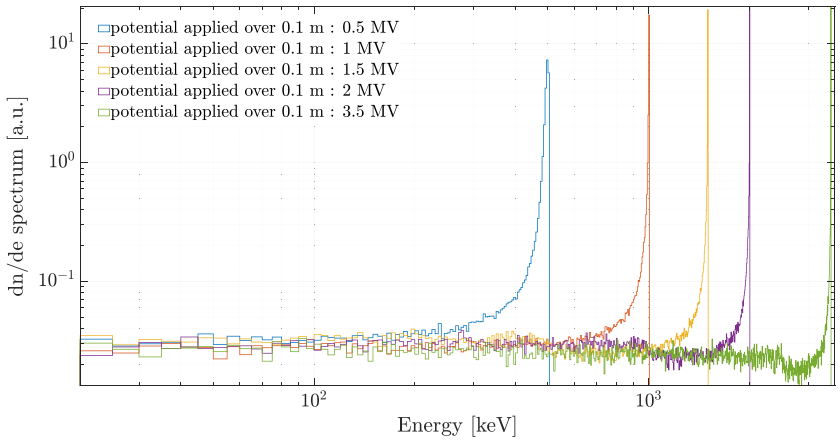

Figure 6. Modeled spectra of 20 keV seed electrons accelerated 0.5, 1, 1.5, 2, and 3.5 MV potentials over a 10 cm distance.

4. Method and Modeling

Our modeling efforts to find the potential difference in the gap between the recoil leader and aircraft, and recoil leader lengths are performed in three steps: (1) a GEANT4 model of the acceleration of 20 keV seed electrons over a small length analogue to the streamer zone, to ascertain if the electrons would all be accelerated to the full applied potential. (2) A second GEANT4 model of the detector and aircraft to model the X-ray spectra that should be detected with the various accelerated electrons from the first GEANT4 model as the input. We then use these modeled spectra to find the best fits to the superposed X-ray spectrum. (3) An electrostatic conductor model (ECM) of a converging lightning leader and aircraft in an ambient electric field, to obtain the potential in the gap between them. Using the potentials found from the second GEANT4 model as potential limits, together with the results of the ECM model and the time difference between the onset of the X-ray bursts and the onset of the currents, we find a solution space for the gap and recoil leader length limited by the lowest potential fit.

4.1. GEANT4 Model 1

A GEANT4 model (Agostinelli et al., 2003; Allison et al., 2006, 2016) was made to model the acceleration of electrons for different potentials over a short distance, analog to the streamer zone, to ascertain if the electrons would be accelerated to the full applied potential. In this model, we start with 20 keV seed electrons (we assume that the electrons have attained this energy from cold runaway, but we do not model this mechanism ourselves). We accelerated the electrons in an electric field that extend over 10 cm. Figure 6 shows the modeled electron spectra of the 20 keV seed electrons accelerated by potentials from 500 to 3,500 kV over a 10 cm distance, normalized by seed number. The figure shows that most electrons are accelerated to the full potential. Going forward, we use the accelerated electrons as a source of the observed X-rays in the second GEANT4 model of the Airbus test aircraft, with the ILDAS equipment on board (as previously used by Kochkin et al., 2018).

4.2. GEANT4 Model 2

In the second GEANT4 model, we model and fit the detected X-ray spectra, with the various accelerated electrons from the first GEANT4 model as input. In this model, we have included the response of our instrument with the aircraft fuselage. Considering that most electrons were accelerated to the full potential in the first GEANT4 model, we assume a monoenergetic electron source as input for this second model. The gap between the leader tip and the aircraft nose was set to 17.5 m, which corresponds to the average observed time between the onset of the X-ray bursts and the onset of the current pulse. A change of up to some tens of meters in the gap distance would not significantly affect the results of this model as it would be much less than the photons mean free path at 4 km altitude in air. In order for the X-rays to reach the detector, the initial electrons have to be within an approximately 20° half angle cone. Outside of this cone, the probability to observe an X-ray photon from the seed electrons is negligible. Therefore, only electrons within the

Table 1
Constant Parameters Used in the Modeling of the Electric Field and Potential Between the Approaching Negative Recoil Leader and the Aircraft

$r_{c.core}$ [m]	$r_{aircraft}$ [m]	$L_{aircraft}$ [m]	$E_{ambient}$ [kV/m]	$Q_{leaders}$ [C]	Altitude scaling factor
0.1	3	67	−24	0	~0.607

Note. r is the conductive core/aircraft radius, L is the aircraft length, E is the assumed ambient electric field, and Q is the assumed leader charge.

half-angle cone were modeled. For the smallest gap distance we use, it is possible for electrons to reach the aircraft itself and interact with the fuselage and detector; this is accounted for in the model.

4.3. ECM Model

A model of the electric field, potential, and charge transferred between the aircraft and the approaching negative leader was created, using the method of moments code as described in Harrington (1993) and Skeltved et al. (2017). The method of moments allows electrostatic modeling of an axially symmetric system of conductors. Multiple disconnected conductors were modeled by having the corresponding number of constraints as a part of the system of equations A4 in Skeltved et al. (2017), which fix the total charge on each of the conductors. The rest of the system is obtained by minimization of the function A5 in Skeltved et al. (2017). The minimization with constraints requires use of Lagrange multipliers, which are the unknown potentials at each of the conductors. When the two disconnected conductors (aircraft and approaching negative leader) electrically connect, their potentials will equalize, while the sum of the charges will stay the same (mathematically, this means that the two constraints become a single constraint). This causes a charge transfer from the conductor that previously had the higher potential to the one with the lower potential. We model both the approaching negative leader and the aircraft as conducting cylinders with hemispherical caps at both ends, with a shared axis of symmetry. The leader channel during the recoil process is analogous to that of a return stroke in cloud-to-ground lightning and has a highly conductive core, with a conductive corona sheath of several meter diameter around it (Lehtinen, 2012). The length and position of the negative recoil leader in the model is variable, while the constant parameters are shown in Table 1.

In the model, we use a leader with conductive core radius of 10 cm, which is somewhat wider than the commonly accepted width of a leader channel; this radius was used because there is high conductivity also around the channel in the corona sheet. To check the results, a conductive core radius of 1 cm was also modeled, in which case the resulting gap potentials showed a mean difference less than 0.1%. The model does not take into consideration the corona sheath, same as in Skeltved et al. (2017). The aircraft is modeled as a conductive cylinder of 67 m length and 3 m radius, which is the actual length and radius of the Airbus A350-900 test aircraft. As the ambient electric field was not measured during the ILDAS campaign, we have chosen to set the value to −24 kV/m. This is the streamer propagation field, scaled to 4 km altitude (average flight altitude) using the scale height of Earth's atmosphere and reduced by a factor of 10, which corresponds to the amplification caused by the geometry of the aircraft (calculated from the ECM model). The initial charges of both the aircraft and the leader were set to zero, as we neglect them compared to the charge separation on both the leader and the aircraft, due to the ambient electric field. These assumptions may slightly affect the gap potential. Figure 7 shows the modeled electric field in the gap between the incoming negative recoil leader and the aircraft. Using the modeled electric field in the gap, we calculate the potential difference between the two leaders for gap distances between 1 and 93 m (from the minimum and maximum time between the onset of the X-ray bursts and the onset of the current pulses) and various recoil leader lengths.

5. Results

An important constraint is the time between the onset of the X-ray observations and the onset of the current pulse through the aircraft, which varies from 0.1 to 9.3 μs, with an average value of 1.75 μs. We assume that the recoil leader speed is similar to that of a dart leader, 10^7 m/s (Howard et al., 2010; Mazur & Moreaut, 1992; Rakov & Uman, 2003), as both leaders are initiated and propagate through an already existing semiconductive channel. From this time span and a recoil leader speed of 10^7 m/s, we get a gap distance between the recoil leader and aircraft ranging from 1 to 93 m, with an average gap distance of 17.5 m. Using the GEANT4 model, we simulate X-ray spectra from electrons accelerated in the average gap of 17.5 m between the aircraft and the recoil leader, to get the spectral shapes for the different potentials. This was done using different leader-to-aircraft potentials ranging from 500 to 1,000 kV in steps of 250 kV and from 1,000 to 4,000 kV in steps of 500 kV.

Figure 8 shows the modeled spectra (dotted lines) for 500, 750, 1,000, 1,500, 2,000, 2,500, 3,000, 3,500, and 4,000 kV potentials in the top panel. The bottom panel shows the results of a likelihood analysis in black,

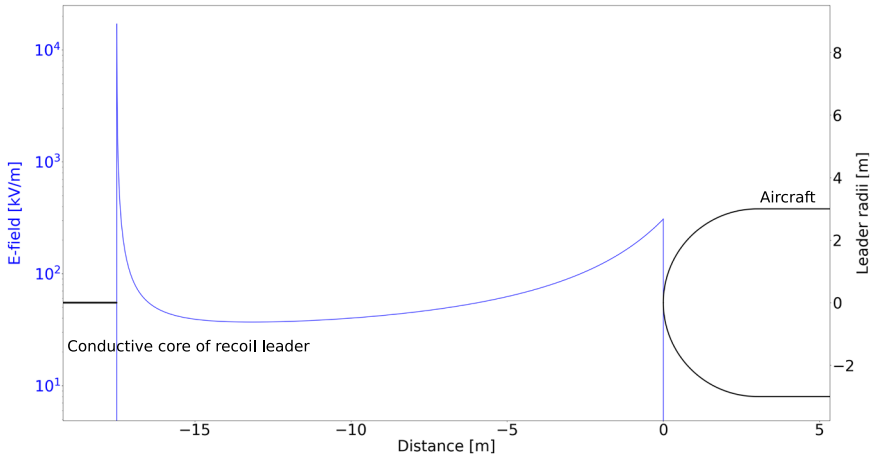

Figure 7. Electric field between lightning leader (left side) and aircraft (right side) in a 17.5 m gap, at 4 km altitude in a −24 kV/m ambient electric field.

performed as in Mailyan et al. (2016); see their Equation 1. According to this test, the best fit is given by minimizing −2log(L), and a difference in −2log(L) larger than 5 means that the minimum value, in this case 1,500 kV, is the preferred solution with a confidence level of 99%, compared to the values above 5 (the dotted black line). We consider all the solutions below the dotted line to be possible solutions (1,000 to 3,500 kV). In the plot, the black line is showing the calculated −2log(L) values subtracted by the minimum −2log(L) value. The bottom panel shows the values of the Pearson χ^2 test in blue (Hauschild & Jentschel, 2001). The test has a critical value of 12.6 (using a 95% threshold) shown as a dotted blue line. The test indicates that the models with potentials between 1,500 and up to 3,500 kV are good fits to our measured data. Due to instrumental limitations, only energies over 50 keV were included in the modeling and calculations of the fits. When calculating the Pearson χ^2 value, we have merged the 300 to 400 keV and the 400 to 500 keV bins, to get at least five measured counts in each bin (Eadie et al., 1971). The modeling also shows X-ray counts over 500 keV, which we have included in a large bin spanning from 500 to 4,000 keV. The calculated Pearson χ^2 values are not dependent on the size of the bins, and as such, the difference in bin widths does not affect the χ^2 value. The minimum potential to yield a fit was found to be 1,500 kV for the Pearson χ^2 analysis, while the likelihood analysis results in a minimum potential of 1,000 kV. As seen in Figure 8, the Pearson χ^2 value crosses the target threshold a bit before 1,500 kV, but we have chosen to use 1,500 kV as the lowest potential fit as this is the first tested value under the target threshold. The maximum potential to yield a fit was found to be 3,500 kV for both Pearson χ^2 and the likelihood analysis.

Using the GEANT4 model, we also estimate the number of 20 keV electrons needed to produce a single detected bremsstrahlung photon of minimum 50 keV for the different source potentials, within the 20° half angle. In a 1,500 kV potential, approximately 1.5×10^9 electrons were needed, while for a 3,500 kV potential, the amount of electrons needed is reduced to approximately 1.1×10^8. The calculated luminosity for the observed recoil leaders with minimum energies of 50 keV are then found to vary from 2.8×10^8 electrons per microsecond for the 3,500 kV source potential up to 3.9×10^9 electrons per microsecond for electrons accelerated in the 1,500 kV source potential.

Using the ECM model, we estimate the relationship of the gap potential and the recoil leader lengths for certain chosen gap distances. This is done by keeping the gap distances fixed and adjusting the recoil leader length. The increase in length results in an increase of the gap potential. Figure 9 shows the relationship between the estimated gap potentials and recoil leader lengths for gap distances between 1 and 75 m, shown by the solid colored lines. The dotted black lines represent the minimum and maximum fit potentials (1,000 and 3,500 kV) found from the GEANT4 model that fit the observed spectrum.

From the intersects of the potential fits found from the GEANT4 model and the solid lines, we find the relationship between the gap and leader lengths for a given source potential. Figure 10 shows the relationship

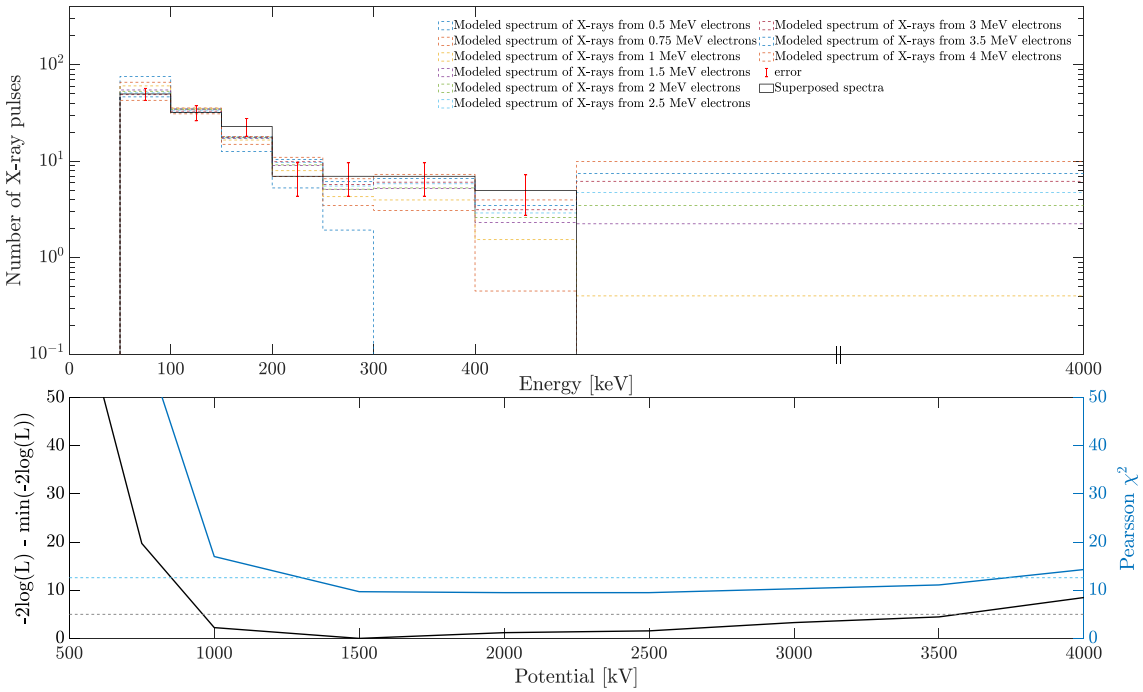

Figure 8. (Top) Observed (black) and modeled (dotted) X-ray spectra with minimum energies of 50 keV, with accompanying error bars in red. The modeled spectra sources are 500, 1,000, 1,500, 2,000, 2,500, 3,000, 3,500, and 4,000 keV electrons, accelerated in a 17.5 m gap between the recoil leader and the aircraft. (Bottom) Fit values for Pearson χ^2 and likelihood analysis, with accompanying dotted lines representing the target values.

between the gap and leader length for 1,500, 2,000, 2,500, 3,000, and 3,500 kV potentials, where the dotted line represents the average measured gap distance calculated from the time between the onset of the X-ray observation and the onset of the current pulse.

6. Discussion

The observed X-ray emissions are all found to be associated with the onset of recoil leaders during aircraft-triggered lightning. A total of 54 X-ray emissions was found, where the emissions consist of submicrosecond bursts of nanosecond-short X-ray pulses. The average burst lasts for ~2 μs and consists of ~4.5 pulses, which is similar to the observations reported by Dwyer et al. (2004), who found submicrosecond bursts of X-rays associated with dart leaders in rocket-triggered lightning. The measured energy spectra extend up to 500 keV, with an average energy ~130 keV. X-rays with higher energies are ruled out, and not included as the few cases where these have been found the measured width of the X-ray pulse is found to be broader than for the calibration pulses, indicating that these X-ray pulses most likely consist of multiple X-rays of lower energies detected within a single sample period.

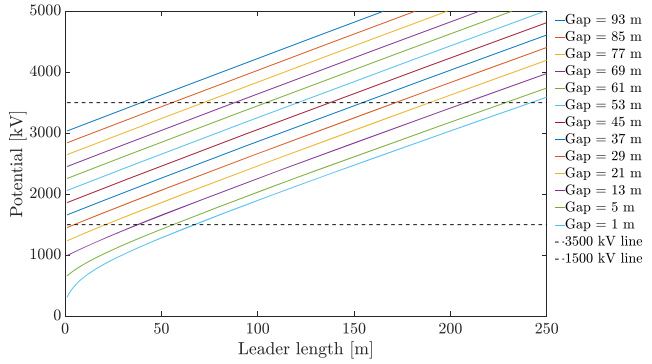

Figure 9. Gap potential as a function of leader length at different gap lengths. The dotted lines represent potentials of 1,500 and 3,500 kV, which is the minimum and maximum potential found to fit the superposed X-ray spectrum.

For the GEANT4 X-ray spectrum, we assumed a recoil leader speed similar to that of a dart leader as both are leaders developing in an already existing conductive lightning channel. With a recoil leader speed of 10^7 m/s combined with the average observed duration between the onset of the X-rays and the onset of the current pulse gives us a gap distance of 17.5 m. The time delays between the onset of the X-ray emissions and the onset of the current pulse vary from 0.1 to 9.3 μs, where the majority of events have delays of less than 2 μs. With the assumed recoil leader speed, this would make the gap distance between 1 and 93 m, with the majority of events having gap distances less than 20 m. As the measured

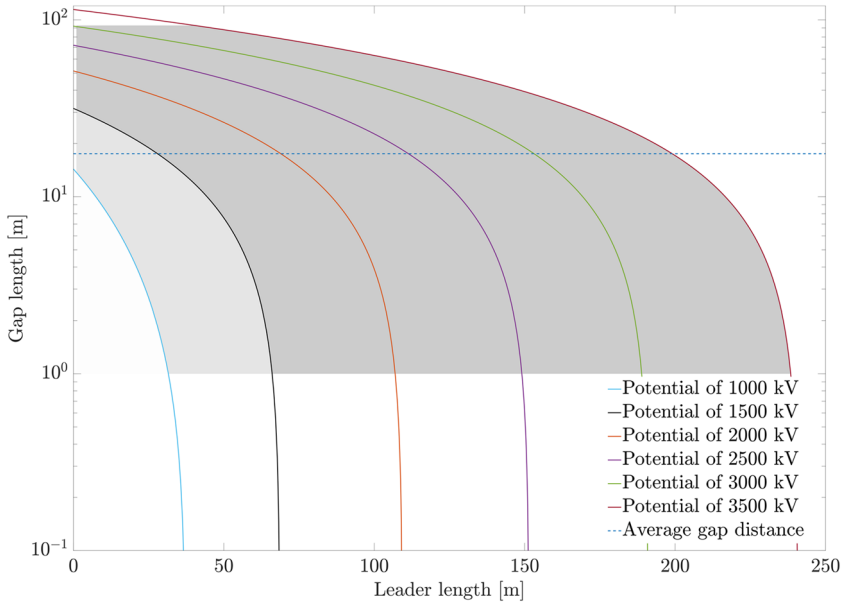

Figure 10. Potential limitations of the gap and leader lengths. The colored lines symbolize the potentials found to fit the superposed spectrum (1,000 up to 3,500 kV) from the second GEANT4 model. The gray areas represent our solution spaces with gap distances restricted by the minimum and maximum measured time between the onset of the X-rays and the onset of the current pulses, as well as the minimum and maximum potential found to fit the superposed spectrum (black/blue and red line). The light gray area is only valid from the likelihood analysis, while the darker gray area is valid for both the likelihood and Pearson χ^2 analysis. The dotted blue line represents the average gap distance also found from the time between onset times.

gap distance is only an indication of the distance to the X-ray source, we cannot conclude that this is the location of the recoil leader head. However, the recoil leader head is the most likely candidate to produce the observed X-rays, and the gap distance is therefore used as the location of the recoil leader head in our models. Changing the gap distance toward either the minimum or maximum value would result in a change of the hardness of the GEANT4 spectra, as the amount of air the X-rays would travel trough would change. Another factor that would lead to a softer spectrum is if the X-rays were not produced by a monoenergetic source of electrons; however as seen in Figure 6, the majority of the modeled source electrons are accelerated to the full potential for a length equal to the assumed leader radius.

From our comparison of the measured X-ray spectrum to the GEANT4 X-ray spectra, we observe that the source of the X-rays is consistent with bremsstrahlung from electrons accelerated in potentials between 1,000 (likelihood)/1,500 (Pearson χ^2) and 3,500 kV. Based on the electron energies, it is thought that the initial seed electrons needed to produce the observed X-rays are most likely accelerated by the strong electric field in front of the recoil leader and streamers (cold runaway mechanism) as the leader travels back through the still conductive, but somewhat cooled leader channel toward the aircraft (Dwyer, 2004; Moss et al., 2006). The calculated electron luminosity for the X-ray source was found to be 3.9×10^9 electrons per microsecond for the minimum potential of 1,500 kV and 2.8×10^8 electrons per microsecond for the best fit potential of 3,500 kV, which is similar to what Saleh et al. (2009) and Schaal et al. (2012) report for X-ray sources in stepped and dart stepped leaders in rocket-triggered lightning. The calculated electron luminosities of the events are based on the assumption that the X-rays are emitted isotropically within the 20° half angle cone; if the emissions were completely isotropic, it would change the calculated luminosities, but it would not affect the modeled spectra and therefore not affect the constraint of the gap and leader lengths.

From the cutoff value in the superposed energy spectrum, we find that there is a limited amount of potentials from the second GEANT4 model that will fit the superposed spectrum. As the modeled potentials increase, so does the amount of modeled X-rays with energies over 500 keV, which increases our Pearson χ^2 and likelihood analysis values over the target values.

In Figure 10, we find a solution space for viable leader lengths and gap lengths. In the figure, the gap distances are constrained by the observed minimum and maximum times between the onset of the X-ray bursts and the onset of the current pulses (1 to 93 m with the assumed dart leader speed of 10^7 m/s). Furthermore, the solution space has a lower and upper constraint found from the lowest and highest potential fit from the second GEANT4 model. These potentials limit the leader length to between 1 and ~240 m. Together, these four constraints limit our solution space to the gray-shaded areas. The model does not give a preferred solution within this solution space; however, from the average time between the onset of the X-ray bursts and the onset of the current pulses, we find the average gap distance (dotted blue line) to be 17.5 m, which limits the average leader length to between ~1 (likelihood)/25 (Pearson χ^2) to 200 m depending on selection of fitting method.

Data Availability Statement

The supporting data used in this paper are published on Zenodo (http://doi.org/10.5281/zenodo.3878590).

Acknowledgments

This study was supported by the European Research Council under the European Union's Seventh Framework Programme (FP7/2007–2013)/ERC Grant Agreement 320839 and the Research Council of Norway under Contracts 208028/F50 and 223252/F50.

References

Agostinelli, S., Allison, J., Amako, K., Apostolakis, J., Araujo, H., Arce, P., et al. (2003). Geant4—A simulation toolkit. *Nuclear Instruments and Methods in Physics Research Section A: Accelerators, Spectrometers, Detectors and Associated Equipment*, *506*(3), 250–303. https://doi.org/10.1016/S0168-9002(03)01368-8

Allison, J., Amako, K., Apostolakis, J., Araujo, H., Arce Dubois, P., Asai, M., et al. (2006). Geant4 developments and applications. *IEEE Transactions on Nuclear Science*, *53*(1), 270–278. https://doi.org/10.1109/TNS.2006.869826

Allison, J., Amako, K., Apostolakis, J., Arce, P., Asai, M., Aso, T., et al. (2016). Recent developments in Geant4. *Nuclear Instruments and Methods in Physics Research Section A: Accelerators, Spectrometers, Detectors and Associated Equipment*, *835*, 186–225. https://doi.org/10.1016/j.nima.2016.06.125

Boissin, J. F., Flourens, F., de Boer, A., Bardet, M., Herve, A., Perez, G., & Riccio, L. (2012). In-flight lightning measurements and reconstruction on a metallic and composite aircraft, 2012 ESA Workshop on Aerospace EMC, Venice, pp. 1–6.

de Boer, A., Bardet, M., Boissin, J. F., van Deursen, A. P. J., Flourens, F., & Herve, A. (2013). In-flight Lightning Damage Assessment System (ILDAS): Further in-flight verification, with multi-sensor configuration. *Proceedings of the 2013 International Conference on Lightning and Static Electricity (ICOLSE), 18–20 September 2013, Seattle, Washington. Conference paper*.

de Boer, A., Bardet, M., Escure, C., Peres, G., Srithammavanh, V., Abboud, K., et al. (2011). In-flight Lightning Damage Assessment System (ILDAS): Initial in-flight lightning tests and improvement of the numerical methods. *Proceedings of the International Conference on Lightning and Static Electricity 2011 (ICOLSE 2011), 6-8 September 2011, Oxford, UK. Conference paper*.

de Boer, A., Boissin, J. F., van Deursen, A. P. J., Flourens, F., Herve, A., & Zwemmer, R. (2013). In-flight Lightning Damage Assessment System (ILDAS): In-flight verification of multi-sensor measurement. *Proceedings of the 2013 International Conference on Lightning and Static Electricity (ICOLSE), 18–20 September 2013, Seattle, Washington. Conference paper*.

de Boer, A., Flourens, F., Herv, A., Bardet, M., & Boissin, J. F. (2015). ILDAS2: From the laboratory to operations—Benefits and performance of the In-flight Lightning Damage Assessment System in support of flight test campaigns. *Proceedings of the 2015 International Conference on Lightning and Static Electricity (ICOLSE 2015), 9–11 September 2015, Toulouse, France. Conference paper*. https://doi.org/10.1049/ic.2015.0198

Deursen, A. (2011). Inductive sensor for lightning current measurement, fitted in aircraft windows—Part II: Measurements on an a320 aircraft. *Sensors Journal, IEEE*, *11*, 205–209. https://doi.org/10.1109/JSEN.2010.2055559

Dwyer, J. R. (2003). Energetic radiation produced during rocket-triggered lightning. *Science*, *299*, 694–698.

Dwyer, J. R. (2004). Implications of X-ray emission from lightning. *Geophysical Research Letters*, *31*, L12102. https://doi.org/10.1029/2004GL019795

Dwyer, J. R., Rassoul, H. K., Al-Dayeh, M., Caraway, L., Chrest, A., Wright, B., & Kozak, E. (2005). X-ray bursts associated with leader steps in cloud-to-ground lightning. *Geophysical Research Letters*, *32*, L01803. https://doi.org/10.1029/2004GL021782

Dwyer, J. R., Rassoul, H. K., Al-Dayeh, M., Caraway, L., Wright, B., & Chrest, A. (2004). Measurements of X-ray emission from rocket-triggered lightning. *Geophysical Research Letters*, *31*, L12102. https://doi.org/10.1029/2004GL019795

Dwyer, J. R., Schaal, M., Rassoul, H. K., Uman, M. A., Jordan, D. M., & Hill, D. (2011). High-speed X-ray images of triggered lightning dart leader. *Journal of Geopysical Research*, *116*, D20208. https://doi.org/10.1029/2011JD015973

Dwyer, J., Smith, D., & Cummer, S. (2012). High-energy atmospheric physics: Terrestrial gamma-ray flashes and related phenomena. *Space Science Reviews*, *173*, 133–196.

Eadie, W. T., Drijard, D., James, F. E., Roos, M., & Sadoulet, B. (1971). *Statistical methods in experimental physics*. Amsterdam: North-Holland Publishing.

Fisher, B. D., Brown, P. W., Plumer, J. A., & Wunschel, A. J. Jr. (1988). Final results of the NASA storm hazards program. *Proceedings of the 1988 International Conference on Lightning and Static Electricity (ICOLSE 1988), 19–21 April 1988, Oklahoma City, Oklahoma. Conference paper*.

Harrington, R. F. (1993). *Field computation by moment methods*. New Jersey: IEEE Press.

Hauschild, T., & Jentschel, M. (2001). Comparison of maximum likelihood estimation and chi-square statistics applied to counting experiments. *Nuclear Instruments and Methods in Physics Research Section A: Accelerators, Spectrometers, Detectors and Associated Equipment*, *457*(1-2), 384–401. https://doi.org/10.1016/S0168-9002(00)00756-7

Hervé, A., Peres, G., de Boer, A., Bardet, M., Flourens, F., & Boissin, J. F. (2014). In-flight Lightning Damage Assessment System (ILDAS): Diagnostic performance assessment with in-fight lightning data. *2014 International Symposium on Electromagnetic Compatibility, 1-4 September 2014, Gothenburg, Sweden* (pp. 589–594). Institute of Electrical and Electronics Engineers. https://doi.org/10.1109/EMCEurope.2014.6930974

Howard, J., Uman, M. A., Biagi, C., Hill, D., Jerauld, J., Rakov, V. A., et al. (2010). RF and X-ray source locations during the lightning attachment process. *Journal of Geophysical Research*, *115*, D06204. https://doi.org/10.1029/2009JD012055

Kelley, N., Smith, D. M., Dwyer, J. R., Splitt, M., Lazarus, S., Martinez-McKinney, F., et al. (2015). Relativistic electron avalanches as a thunderstorm discharge competing with lightning. *Nature Communications*, *6*, 1–7. https://doi.org/10.1038/ncomms8845

Kochkin, P., Sarria, D., Skeie, C. A., van Deursen, A. P. J., de Boer, A. I., Bardet, M., et al. (2018). In-flight observation of positron annihilation by ILDAS. *Journal of Geophysical Research: Atmospheres*, *123*, 8074–8090. https://doi.org/10.1029/2018JD028337

Kochkin, P., van Deursen, A. P. J., de Boer, A., Bardet, M., & Boissin, J.-F. (2015). In-flight measurements of energetic radiation from lightning and thunderclouds. *Journal of Physics D: Applied Physics*, *48*, 425,202. https://doi.org/10.1088/0022-3727/48/42/425202

Kochkin, P., van Deursen, A. P. J., Marisaldi, M., de Boer, A. I., Bardet, M., Allasia, C., et al. (2017). In-flight observation of gamma ray glows by ILDAS. *Journal of Geophysical Research: Atmospheres*, *122*, 12,801–12,811. https://doi.org/10.1002/2017JD027405

Lalande, P., Bondiou-Clergerie, A., & Laroche, P. (1999). Analysis of available in-flight measurements of lightning strikes to aircraft. *SAE Technical Paper Series*, *724*. https://doi.org/10.4271/1999-01-2397

Laroche, P., Blanchet, P., Delannoy, A., & Issac, F. (2012). Experimental studies of lightning strikes to aircraft. *Aerospace Lab Journal*, *5*, 1–13.

Lehtinen, N. G. (2012). A waveguide model of the return stroke channel with a "metamaterial" corona. *Radio Science*, *47*, RS1003. https://doi.org/10.1029/2011RS004749

Mailyan, B. G., Briggs, M. S., Cramer, E. S., Fitzpatrick, G., Roberts, O. J., Stanbro, M., et al. (2016). The spectroscopy of individual terrestrial gamma-ray flashes: Constraining the source properties. *Journal of Geophysical Research: Space Physics*, *121*, 11,346–11,363. https://doi.org/10.1002/2016JA022702

Mazur, V. (1989a). A physical model of lightning initiation on aircraft in thunderstorms. *Journal of Geophysical Research*, *94*, 3326–3340. https://doi.org/10.1029/JD094iD03p03326

Mazur, V. (1989b). Triggered lightning strikes to aircraft and natural intracloud discharges. *Journal of Geophysical Research*, *94*(D3), 3311–3325. https://doi.org/10.1029/JD094iD03p03311

Mazur, V. (2002). Physical processes during development of lighting flashes. *Applied Physics*, *3*, 1393–1409. https://doi.org/10.1016/S1631-0705(02)01412-3

Mazur, V., & Moreaut, J. P. (1992). Aircraft-triggered lightning: Processes following strike initiation that affect aircraft. *Journal of Aircraft*, *29*(4), 575–580. https://doi.org/10.2514/3.46204

Mazur, V., & Ruhnke, L. H. (1993). Common physical processes in natural and artificially triggered lightning. *Journal of Geophysical Research*, *98*, 12,913–12,930. https://doi.org/10.1111/j.1555-2934.2009.01042.x

Mazur, V., Ruhnke, L. H., Warner, T. A., & Orville, R. E. (2013). Recoil leader formation and development. *Journal of Electrostaticss*, *71*, 763–768. https://doi.org/10.1016/j.elstat.2013.05.001

McCarthy, M., & Parks, G. K. (1985). Further observations of X-rays inside thunderstorms. *Geophysical Research Letters*, *12*, 393–396. https://doi.org/10.1029/GL012i006p00393

Miller, E. (1968). Synopsis of a thunderstorm research program (Roughrider) for 1966–1967 (*Technical Report ASD-TR-68-29*).

Montanyà, J., Fabró, F., van der Velde, O., Romero, D., Solà, G., Hermoso, J. R., et al. (2014). Registration of X-rays at 2500 m altitude in association with lightning flashes and thunderstorms. *Journal of Geophysical Research: Atmospheres*, *119*, 1492–1503. https://doi.org/10.1002/2013JD021011

Moore, C. B., Eack, K. B., Aulich, G. D., & Rison, W. (2001). Energetic radiation associated with lightning stepped-leaders. *Geophysical Research Letters*, *28*, 2141–2144. https://doi.org/10.1029/2001GL013140

Moreaut, J. P., Alliot, J. C., & Mazur, V. (1992). Aircraft lightning initiation and interception from in situ electric measurements and fast video observations. *Journal of Geophysical Research*, *97*(D14), 15,903–15,912. https://doi.org/10.1029/92JD01077

Moss, G. D., Pasko, V. P., Liu, N., & Veronis, G. (2006). Monte Carlo model for analysis of thermal runaway electrons in streamer tips in transient luminous events and streamer zones of lightning leaders. *Journal of Geophysical Research*, *111*, A02307. https://doi.org/10.1029/2005JA011350

Ogawa, T., & Brook, M. (1964). The mechanism of the intracloud lightning discharge. *Journal of Geophysical Research*, *69*(24), 5141–5150. https://doi.org/10.1029/JZ069i024p05141

Østgaard, N., Christian, H. J., Grove, J. E., Sarria, D., Mezentsev, A., Kochkin, P., et al. (2019). Gamma ray glow observations at 20-km altitude. *Journal of Geophysical Research: Atmospheres*, *124*, 7236–7254. https://doi.org/10.1029/2019JD030312

Parks, G. K., Mauk, B. H., Spiger, R., & Chin, J. (1981). X-ray enhancements detected during thunderstorm and lightning activities. *Geophysical Research Letters*, *8*, 1176–1179. https://doi.org/10.1029/GL008i011p01176

Rakov, V. A., & Uman, M. A. (2003). *Lightning: Physics and effects*. Cambridge: Cambridge University Press.

Royal Netherlands Aerospace Laboratory (2015). Accurate measurements during multiple lightning strikes. https://ildas.nlr.nl/

Saleh, Z., Dwyer, J., Howard, J., Uman, M., Bakhtiari, M., Concha, D., et al. (2009). Properties of the X-ray emission from rocket-triggered lightning as measured by the Thunderstorm Energetic Radiation Array (TERA). *Journal of Geophysical Research*, *114*, D17210. https://doi.org/10.1029/2008JD011618

Schaal, M. M., Dwyer, J. R., Saleh, Z. H., Rassoul, H. K., Hill, J. D., Jordan, D. M., & Uman, M. A. (2012). Spatial and energy distributions of X-ray emissions from leaders in natural and rocket triggered lightning. *Journal of Geophysical Research*, *117*, D15201. https://doi.org/10.1029/2012JD017897

Skeltved, A. B., Østgaard, N., Mezentsev, A., Lehtinen, N., & Carlson, B. (2017). Constraints to do realistic modeling of the electric field ahead of the tip of a lightning leader. *Journal of Geophysical Research: Atmospheres*, *122*, 8120–8134. https://doi.org/10.1002/2016JD026206

Uman, M. A., & Rakov, V. A. (2003). The interaction of lightning with airborne vehicles. *Progress in Aerospace Sciences*, *39*(1), 61–81. https://doi.org/10.1016/S0376-0421(02)00051-9

van Deursen, A. P. J., de Boer, A., Bardet, M., & Boissin, J. F. (2013). Window sensor for the a350 and a380 aircraft, *2013 International Conference on Electromagnetics in Advanced Applications (ICEAA)* (pp. 1000–1003).

Zwemmer, R., Bardet, M., de Boer, A., Hardwick, J., Hawking, D. K. M., Latorre, M., et al. (2009). In-flight Lightning Damage Assessment System (ILDAS); results of the concept prototype tests. *Proceedings of the 2009 International Conference on Lightning and Static Electricity (ICOLSE), 15–17 September 2009, Pittsfield, Massachusetts. Conference paper*.